Introgression between highly divergent sea squirt genomes: an adaptive breakthrough?

Christelle Fraïsse[1,2,*], Alan Le Moan[3,4], Camille Roux[1], Guillaume Dubois[3], Claire Daguin-Thiébaut[3], Pierre-Alexandre Gagnaire[2], Frédérique Viard[2,3,°], Nicolas Bierne[2,°]

[1] CNRS, Univ. Lille, UMR 8198 – Evo-Eco-Paleo, F-59000 Lille, France.

[2] ISEM, Univ Montpellier, CNRS, EPHE, IRD, Montpellier, France

[3] CNRS UMR 7144 - Sorbonne University, 29680 Roscoff, France.

[4] Department of Marine Sciences, Tjärnö Marine Laboratory, University of Gothenburg, 452 96 Strömstad, Sweden.

[*]Corresponding author: E-mail: christelle.fraisse@univ-lille.fr

[°]Co-last authors

Keywords: ascidians, trio-based genome phasing, anthropogenic hybridization, introgression hotspot, cytochrome P450.

Short title: Adaptive breakthrough in sea squirts

Abstract

Human-mediated introductions are reshuffling species distribution on a global scale. Consequently, an increasing number of allopatric taxa are now brought into contact, promoting introgressive hybridization between incompletely isolated species and new adaptive gene transfer. The broadcast spawning marine species, *Ciona robusta*, has been recently introduced in the native range of its sister taxa, *Ciona intestinalis*, in the English Channel and North-East Atlantic. These sea squirts are highly divergent, yet hybridization has been reported by crossing experiments and genetic studies in the wild. Here, we examined the consequences of secondary contact between *C. intestinalis* and *C. robusta* in the English Channel. We produced genomes phased by transmission to infer the history of divergence and gene flow, and analyzed introgressed genomic tracts. Demographic inference revealed a history of secondary contact with a low overall rate of introgression. Introgressed tracts were short, segregating at low frequency, and scattered throughout the genome, suggesting traces of past contacts during the last 30 ky. However, we also uncovered a hotspot of introgression on chromosome 5, characterized by several hundred Kb-long *C. robusta* haplotypes segregating in *C. intestinalis*, that introgressed during contemporary times the last 75 years. Although locally more frequent than the baseline level of introgression, *C. robusta* alleles are not fixed, even in the core region of the introgression hotspot. Still, LD patterns and haplotype-based tests suggest this genomic region is under recent positive selection. We further detected in the hotspot an over-representation of candidate SNPs lying on a cytochrome P450 gene with a high copy number of tandem repeats in the introgressed alleles. Cytochromes P450 are a superfamily of enzymes involved in detoxifying exogenous compounds, constituting a promising avenue for functional studies. These findings support that introgression of an adaptive allele is possible between very divergent genomes and that anthropogenic hybridization can provide the raw material for adaptation of native lineages in the Anthropocene.

Author summary

Introgression, the transfer of genetic material by hybridization between taxa, is increasingly recognized to sometimes persist for long during species divergence. However, the evolutionary consequences of human-induced introgression remain largely unknown, especially in the marine realm. While some argue it poses a threat to the genome integrity of native species, others consider it has a great potential to fuel adaptation. In this work, we quantify the magnitude and genomic distribution of introgression after secondary contact between a native sea squirt and its divergently related sister species recently introduced in the English Channel. The genome-wide pattern suggests introgression is mostly impeded between these two incompatible genomes that only exchanged a few very short chromosome tracts sparsely distributed in the native genome. We nonetheless found a hotspot of long tracts that recently introgressed in a single region of the genome, with a clear footprint of recent positive selection. In the center of the hotspot, we further detected a promising candidate gene for adaptive introgression: a cytochrome P450 detoxifying enzyme with a high copy number in the introgressed allele. Therefore, our results support that adaptive introgression can remain possible between very divergent genomes and that anthropogenic hybridization can provide the raw material for the adaptation of native lineages in the Anthropocene.

Introduction

Human-mediated introductions often result in interlineage introgression (North et al. 2021; Ottenburghs 2021). Pervasive introgression implies that most co-occurring introduced and native genomes of sister species are still to some extent permeable to interspecific gene flow, with various outcomes from genome-wide genetic swamping to adaptive introgression at few specific genomic regions (McFarlane and Pemberton 2019). In the marine realm, harbors, docks and piers are prime locations for such hybridization events between non-native and native lineages, sometimes resulting in singular outcomes. For example, (Simon et al. 2020) identified a unique ecotype of marine mussels in these artificial habitats ("docks mussels"), resulting from a recent admixture between two closely-related European mussel species. These anthropogenic hybridizations can also promote secondary contact between divergent genomes with long histories of allopatric divergence (Viard et al. 2020). They provide unique opportunities to investigate the outcomes of hybridization between co-occurring genetic lineages at a late stage of the speciation continuum.

Sea squirts are among the most critical invasive marine organisms forming a significant component of the non-indigenous community in artificial marine habitats (Shenkar and Swalla 2011; Zhan et al. 2015). For this reason, they were among the first marine taxa to be studied to test the hypothesis of the relationship between climate change and biological invasions (Stachowicz et al. 2002). *Ciona robusta* is a sea squirt species native to the Northwest Pacific introduced in the early 2000s to the English Channel in the native range of *Ciona intestinalis* (Bouchemousse, Bishop, et al. 2016). The two species are found in sympatry in these regions (Nydam and Harrison 2011). However, their relative abundance varies locally over seasons (Bouchemousse, Lévêque, et al. 2016), and they display contrasting genetic diversity patterns, with low mitochondrial diversity in *C. robusta* supporting its recent introduction (Bouchemousse, Bishop, et al. 2016). *C. robusta* and *C. intestinalis* represent a pair of species at the end of the speciation continuum with 14% of net synonymous

divergence, which is well above the ~2% suggested to delineate the end of the grey zone of speciation in most animals (Roux et al. 2016). Despite this high molecular divergence, first and second-generation crosses between the two species show successful hybridization in the laboratory (Bouchemousse, Lévêque, et al. 2016; Malfant et al. 2018). Moreover, the two species produce gametes synchronously in the wild, with juveniles recruiting simultaneously (Bouchemousse, Lévêque, et al. 2016). However, the use of >300 ancestry-informative markers on 450 individuals showed limited evidence for recent hybridization in the wild, with only one F1 and no later generation hybrids found in the sympatric range (Bouchemousse, Liautard-Haag, et al. 2016). Therefore, efficient reproductive barriers seem to restrict hybridization in nature.

Despite the paucity of first-generation hybrids, Le Moan et al. (2021) found compelling evidence of contemporary introgression between *C. robusta* and *C. intestinalis* in the sympatric range (Bay of Biscay, Iroise Sea and the English Channel) from RADseq-derived SNPs. Instead of genome-wide admixture, Le Moan et al. (2021) detected a single genomic hotspot (~1.5 Mb) of long introgressed *C. robusta* tracts into its native congener on chromosome 5. The absence of such introgression tracts in allopatric populations suggests introgression occurred after the recent introduction of *C. robusta*. At a fine spatial scale within the sympatric range, the introgressed tracts displayed chaotic frequencies across sympatric localities, which has been attributed to human--mediated transport among harbors (Hudson et al. 2016). The features of the introgression hotspot identified between the two species, namely being 1) unidirectional, 2) localized in a single genome region, and 3) made-up of long tracts, are reminiscent of the footprint of positive selection. Therefore, Le Moan et al.'s work (2021) provides a seminal example of a contemporary introgression breakthrough between two species at a late stage of the speciation continuum. It underlines the need to densely scan genomes with genome-wide markers, notably when considering divergent genomes that may only show very localized introgression hotspots (Ravinet et al. 2018; Maxwell et al. 2019; Stankowski et al. 2020; Yamasaki et al. 2020).

Here, we extend Le Moan et al.'s study (2021) using whole-genome sequences fully phased by transmission in both *C. robusta* and *C. intestinalis* taken from their sympatric range (English Channel), to *i)* specifically delineate the core region of the genomic breakthrough, *ii)* test for the footprint of selection, and *iii)* identify candidate loci driving the putatively adaptive introgression. We also examined a non-introgressed *Ciona roulei* population in the Mediterranean Sea, used as a control. Based on experimental crosses and genome-wide analyses, recent studies showed that *C. roulei* is a "Mediterranean lineage" of the accepted species *C. intestinalis*, and thus its species status needs to be revised (Malfant et al. 2018; Le Moan et al. 2021). However, we will continue to name it "*C. roulei"* in this study. Based on whole genomes, we recovered the observation of Le Moan et al. (2021) for a genomically localized introgression breakthrough on chromosome 5 from *C. robusta* to the sympatric *C. intestinalis*, absent in the *C. roulei* population of the Mediterranean Sea. We also inferred the divergence history of the two species and confirmed that they have hybridized in the past, far before their introduction in Europe (Roux et al. 2013). However, when including chromosome 5, we recovered a signal of contemporary introgression. Next, we inferred the haplotype ancestry of the *C. intestinalis* genomes and delineated migrant genomic tracts. In sharp contrast with a genomic background interspersed with small and sparse introgressed tracts attributed to past admixture, we found a distinct pattern of very long introgressed tracts segregating at intermediate frequencies at the introgression hotspot on chromosome 5. Finally, using haplotype-based tests, we provided evidence that the high linkage disequilibrium (LD) observed in the genomic hotspot is due to some sort of positive selection. Inspecting annotated genes at the core of the introgression breakthrough, our best candidate for selection was a cytochrome P450 gene, on which differentiated SNPs were over-represented, and that showed a high copy number tandem repeat in the *C. robusta* introgressed haplotype.

Results

Genome-wide analysis of population structure

A principal component analysis on genome-wide unlinked SNPs (**Figure 1B**) showed, as expected, that the *C. robusta* individuals are clearly distinguished from the *C. intestinalis* individuals sampled in the sympatric populations of the English Channel (Brest and Aber Wrac'h, named 'Aber' in the following text) and from the non-introgressed population of the Mediterranean Sea (Banyuls, *C. roulei*). This primary component of genetic variation was carried by the first PCA axis (21.2% of explained variance). In comparison, the second axis (6.7%) revealed a slight genetic differentiation between *C. intestinalis* and *C. roulei*, validating previous findings with RADseq (Le Moan et al. 2021). The intraspecific F1 individuals produced in the lab (**Table S1**) fall within the genetic variance of their species, while the interspecific F1s fall halfway between the two species along the first axis (**Figure 1B**), validating their F1 hybrid status. The intraspecific variance along the first axis was substantial within *C. intestinalis.* At the same time, this was not the case of *C. robusta* and *C. roulei*, suggesting that interspecific introgression affects specifically *C. intestinalis* individuals in the English Channel.

The SNPs contributing to species divergence on the first axis are distributed genome-wide (**Figure 1C**). Still, a decline of SNP contribution on the first axis at the start of chromosome 5 indicated a reduction of the divergence between *C. robusta* and the sympatric *C. intestinalis* populations locally in the genome. This pattern is supported by the observation of a consistently high divergence across the genome between *C. robusta* and *C. intestinalis* (the maximal F_{ST} calculated in non-overlapping 10 Kb windows is equal to one), except at the start of chromosome 5, where the maximal F_{ST} value declined from 1 to 0.69 (**Figure S1A**). This striking decline, located between 700 Kb and 1.5 Mb, was not observed between *C. robusta* and *C. roulei* (**Figure S1B**). Moreover, in *C. intestinalis,* it did not correlate with a reduction of diversity (π), suggesting it is likely due to interspecific introgression rather than intraspecific selective sweeps. This pattern is very different from

151 what was observed for the averaged F_{ST} (**Figure S1**) that strongly varied across the genome. It was
152 notably higher at the beginning or in the middle of the chromosomes in regions of low intraspecific
153 genetic diversities. These large-scale averaged variations were observed in all species, indicating that
154 they may be due to the long-term effect of linked selection acting on a shared recombination landscape
155 (note that all chromosomes in *C. intestinalis* are metacentric, except chromosome 2, 7 and 8, which are
156 submetacentric (Shoguchi et al. 2006).

157 Genome-wide analysis of introgression

158 We calculated the Patterson's *D* statistic using *C. edwardsi* as an outgroup to test for genome-wide
159 admixture between the two species (**Figure S4**). We found evidence for an excess shared ancestry of
160 *C. robusta* with the sympatric *C. intestinalis* relative to *C. roulei* across all chromosomes (**Figure S4**).
161 To locate introgressed genomic regions, the fraction of the genome that has been shared between
162 species (*fd*) was then calculated in non-overlapping windows. *fd* varied around zero along each
163 chromosome, but we observed an outlying increase on chromosome 5 between 700 Kb and 1.5 Mb
164 showing a high admixture level between *C. robusta* and *C. intestinalis* (**Figure S4**). This *fd* increase
165 had its maximum (25% of admixture level) centered on the introgression hotspot of chromosome 5 and
166 was only present in the sympatric range. None of the other chromosomes showed outlying genomic
167 regions, neither with *C. intestinalis*, nor with *C. roulei*. Furthermore, the admixture proportion was
168 weakly negatively correlated with chromosome length, a known proxy for the recombination rate
169 (Kaback 1996), but chromosome 5 was a clear outlier (it has a higher *fd* value than expected given its
170 size).

171 We detected introgression tracts in *C. intestinalis* genomes using local ancestry inference on
172 640,044 phased SNPs and considering *C. robusta* and *C. roulei* as the parental populations. The
173 inferred tracts showed similar introgression patterns to the raw haplotypes obtained from SNPs fixed
174 between *C. robusta* and *C. roulei* (**Figure S2**). This suggests that local ancestry inferences indeed
175 detect the introgressed genomic regions while being less noisy than when considering raw haplotypes.

176 The proportion of *C. robusta* ancestry inferred was low (0.1% on average per individual), suggesting
177 that the introgression rate at the genome level is low. Furthermore, there was no significant correlation
178 in *C. robusta* ancestry between chromosomes (except in 5 pairs) among the *C. intestinalis* individuals
179 (**Table S2**). Introgressed tracts were short (median size of 380 bp) and widespread across the genome
180 (**Figure 2**). These short tracts had a bimodal frequency distribution with a majority segregating at low
181 frequency and a minority fixed in *C. intestinalis*. They likely have originated from past admixture
182 events between the two species and then progressively been chopped down by recombination over
183 time while they drifted towards loss or fixation. The introgression hotspot on chromosome 5
184 immediately appears as an outlier on the chromosome map (**Figure 2**). Its underlying tracts were much
185 longer (maximal size of 156 Kb) than the tracts outside of the hotspot, and they segregated at
186 intermediate frequencies (none of the long tracts on the hotspot was fixed), in line with a recent
187 introgression event.

188 We then analyzed the coding sequences inside and outside the genomic tracts identified as
189 being introgressed (**Figure S3**). Chromosome 5 carries by far the largest number of introgressed CDS:
190 65 of 69 were located on this chromosome, while the four other introgressed CDS were located on
191 three different chromosomes (3, 8 and 13). Among all CDS on chromosome 5, 6% were detected as
192 being on introgressed tracts, demonstrating that the hotspot does contain introgressed genes. As
193 introgression has not reached fixation in *C. intestinalis,* we would expect an increase of diversity
194 within *C. intestinalis* (π) and a decrease of interspecies divergence (d_{XY}) for the CDS on introgressed
195 tracts compared to the rest of the genome. However, this is not what was observed (**Figure S3A**),
196 probably because the *C. robusta* introgressed alleles segregate at an intermediate frequency that
197 negligibly impacts diversity. Therefore, we computed the G_{min} statistic, defined as the ratio of the
198 minimum d_{XY} to the average d_{XY}, which is better suited to capture the effect of recent introgression
199 events (Geneva et al. 2015). As expected if introgressed tracts originate from recent introgression

200 events, we found that G_{min} was significantly lower in the introgressed CDS than in the rest of the
201 genome (**Figure S3B**).

202 The history of divergence and gene flow between *C. robusta* and *C. intestinalis*

203 In order to address whether short and long *C. robusta* tracts introgressed in the *C. intestinalis* genomes
204 could result from different introgression events, we reconstructed the divergence history between the
205 two species based on their joint site frequency spectrum. Divergence models in which the history of
206 gene flow can take different forms were tested. The possibilities of having a heterogeneity of effective
207 population sizes and effective migration rates to model the effects of linked selection and species
208 barriers were also included in the models. This is because previous work showed that when these
209 features were not considered, the inferences led to ambiguous results in sea squirts (Roux et al. 2016).
210 We first excluded chromosome 5 from the inferences to capture the prominent history between the two
211 species (**Figure 3** and **Table S3** for details). Divergence with periodic connectivity and the effects of
212 linked selection was the best model, closely followed by a secondary contact model. The divergence
213 between the two species started with gene flow (during ~400 Ky), then it was followed by a ~1.5 My
214 period of isolation. Only in the 30,000 last years, *C. robusta* and *C. intestinalis* came into secondary
215 contact. This long period of introgression could explain the presence of the short introgressed tracts in
216 *C. intestinalis*. In line with this scenario, the estimates of migration rates show that introgression is
217 highly asymmetrical from *C. robusta* toward *C. intestinalis*. Furthermore, we observed a ten-fold
218 lower effective population size in *C. robusta* than *C. intestinalis*, which matches the difference in
219 nucleotide diversities between the two species and can be explained by the recent introduction of *C.*
220 *robusta* in Europe (**Figure S1**). Repeating the demographic analyses with chromosome 5 in the dataset
221 led to very similar parameter estimates, except for the divergence times (**Figure S5** and **Table S4** for
222 details). Indeed, the best model was now a secondary contact, where a long period of isolation (~2
223 My) was followed by a contemporary period of introgression (in the last 200 years), which may
224 capture the signal left by the long introgressed tracts on chromosome 5.

225 We used a neutral recombination clock to refine the time estimate since admixture at the
226 introgression hotspot on chromosome 5. The average length of the introgressed tracts can be estimated
227 using the formula $\bar{L} = [\ (1 - f) * r * (t - 1)\ ]^{-1}$, where r is the local recombination rate (crossovers
228 per base pair per generation), f is the admixture proportion, and t is the time since the admixture event
229 in generations (Racimo et al. 2015). Given that the average length of introgressed tracts at the hotspot
230 is 19,898 bp, the mean frequency of introgression is 0.106, and the recombination rate is 3.82e-07
231 M/bp (Duret, pers. comm.), we found that the contemporary admixture between *C. robusta* and *C.*
232 *intestinalis* occurred about 75 years ago (assuming two generations per year; (Bouchemousse et al.
233 2017). Note that due to small regions lacking sufficient ancestry signal (**Figure S7**), some introgressed
234 tracts could be a bit longer than measured, indicating an even more contemporary introgression.

235 The introgression hotspot on chromosome 5

236 We have shown that maximal F_{ST} values between *C. robusta* and *C. intestinalis* form a valley at the
237 start of chromosome 5 (**Figure 4A**). This pattern is due to long *C. robusta* tracts segregating in the
238 sympatric populations of *C. intestinalis* (**Figure 4B**). The introgression tracts were variable in size.
239 They shared ancestral recombination breakpoints, clearly visible in the linkage disequilibrium (LD)
240 heatmap between pairs of diagnostic SNPs along chromosome 5 (**Figure 4D**). The hotspot region
241 between 700 Kb and 1.5 Mb exhibited stronger LD (r^2 median of 0.3) than the rest of chromosome 5
242 (r^2 median of 0.007). Introgression was maximal on either side of the "missing data region" from
243 1,009,000 to 1,055,000 bp (a region of significantly increased read depth: 100x in average inside the
244 region *vs* 25x outside). But we found no evidence of introgressed tracts in the hotspot that have
245 completely swept to fixation in *C. intestinalis* (**Figure 4C**).

246 To explicitly test if some sort of selection could explain this pattern on chromosome 5, we
247 used various methods. We first sought the footprint of a classic selective sweep, where a *de novo*
248 beneficial mutation arises on a *C. robusta* haplotype and quickly sweeps toward fixation, reducing
249 diversity and creating a signal of long-range LD around it. This signal can be captured by the extended

250 haplotype homozygosity (EHH), which measures the decay of identity-by-descent between haplotypes
251 as a function of the distance from a focal SNP. Taking as targets the SNPs with the highest *C. robusta*
252 frequency to the left and right of the "missing data region", we observed a slower EHH decay on the
253 *C. robusta* haplotypes compared to other haplotypes in the sympatric *C. intestinalis* populations, but
254 not in the *C. roulei* population (**Figure 4E**). To test for significance, the absolute normalized integrated
255 haplotype score (iHS) was then calculated in 50-Kb windows along chromosome 5, and we estimated
256 the proportion of SNPs in each window associated with outlying values of iHS. This proportion was
257 the highest in the core region of the introgression hotspot in *C. intestinalis* (8%) and *C. robusta* (20%),
258 but not in *C. roulei* (0%). This result indicates a low haplotype diversity over an extended region in
259 both the donor *C. robusta* and the introgressed alleles of the recipient *C. intestinalis* populations. The
260 genealogies of the 50-kb windows framing the "missing data region" further support a reduced
261 diversity of the *C. robusta* clade (**Figure S8**). Moreover, the alleles sampled in the introgressed *C.*
262 *intestinalis* genomes cluster within the star-like *C. robusta* clade, suggesting that a recent selective
263 sweep happened in *C. robusta* and a single beneficial haplotype introgressed into *C. intestinalis*.
264 Finally, we used a complementary approach (VolcanoFinder) to directly test for adaptive
265 introgression using all SNPs from the *C. intestinalis* recipient species only. Again, the method is
266 suitable to detect an adaptively introgressed allele that has swept to fixation in the recipient species,
267 producing intermediate-frequency polymorphism in its flanking regions. Although introgression was
268 incomplete in our case (generating a soft sweep pattern, which may lead to a decrease in power), we
269 nonetheless observed a signal of adaptive introgression on the hotspot of chromosome 5 (**Figure S6**).
270 Several other regions in the genome showed extreme values of the log-likelihood ratio test. However,
271 contrary to the introgression hotspot, these regions also displayed signals of *de novo* selective sweeps
272 within *C. intestinalis* (detected with SweepFinder) that globally correlated with genomic regions of
273 reduced diversity (**Figure S1**). In contrast, a signal of *de novo* selective sweep within *C. robusta* was

274 detected in the introgression hotspot, supporting the view that beneficial alleles in this species recently
275 swept to fixation and were adaptively introgressed into the sympatric *C. intestinalis*.

276 Copy number variation at the introgression hotspot

277 We then annotated the introgression hotspot region of chromosome 5 (700 Kb - 1.5 Mb) to identify
278 putative candidate genes under selection. To overcome the difficulty posed by the high coverage of the
279 "missing data region" at the center of the hotspot, we relied on the variant allele fraction (VAF)
280 calculated from read depth to find candidate SNPs. Because the reference genome used throughout this
281 paper is from *C. robusta*, the variant allele represents the alternate allele in the *C. robusta* genome.
282 Candidate SNPs were defined as being differentiated between *C. robusta* and *C. roulei*, therefore
283 having a low VAF in the former and a high VAF in the latter, and being exclusively introgressed in the
284 sympatric *C. intestinalis* (VAF below 50%). Using a lenient threshold of VAF higher than 85% in *C.*
285 *roulei* and below 15% in *C. robusta*, we found 28 candidate SNPs in the 800-Kb region of the hotspot
286 distributed across six different protein-coding genes and two non-coding loci (**Figure S9**). Only
287 variants in the "missing data region" (20 of 28 SNPs) showed a coverage pattern in line with multi-
288 copy genes. Notably, 16 of these SNPs were located on the cytochrome P450 family 2 subfamily U
289 gene. Three other cytochromes from family 2 were found in the "missing data region" (subfamilies J/
290 D/R; **Figure S10**), but none contained candidate SNPs.

291 We did not find candidate SNPs where the *C. robusta* allele had swept to fixation in *C.*
292 *intestinalis*. The SNP showing the highest introgression frequency (0.85, i.e., only two non-
293 introgressed *C. intestinalis* individuals out of 13 sampled) was located in a single-copy non-coding
294 locus at position 1,067,404 bp. Nevertheless, this pattern should be interpreted with caution as many
295 individuals had a shallow read depth at this SNP. Considering the multi-copy genes, the 16 variants on
296 the cytochrome P450 all exhibited the same pattern of a high copy number of the introgressed *C.*
297 *robusta* allele, while this was not the case of the other multi-copy genes (**Figure S9**). Two candidate
298 SNPs on the cytochrome P450 are represented in **Figure 5**. They showed that *C. robusta* individuals

299 carried from five to twenty copies of the reference allele, while *C. roulei* individuals had one or two
300 copies of the alternate allele. As for the introgressed *C. intestinalis*, they were heterozygous with one
301 copy of the *C. intestinalis* allele and at least ten copies of the *C. robusta* allele, while the non-
302 introgressed *C. intestinalis* individuals were like *C. roulei*. This pattern suggests the presence of
303 multiple copies in tandem repeats of the *C. robusta* allele on cytochrome P450, which might play a
304 critical role in adaptation, and have favored its introgression into *C. intestinalis*.

305 Discussion

306 We used phased genomes from whole-genome trio sequencing to document the fine-scale genomic
307 consequences of the human-mediated contact between the invasive *C. robusta* and the native *C.*
308 *intestinalis* sea squirt species in Europe. A Mediterranean *C. roulei* population was also whole-genome
309 sequenced to be used as a non-introgressed control. Despite their high divergence, we have
310 demonstrated that the introduced and native species still hybridize in their sympatric range, showing a
311 localized introgression hotspot in the native species. We provided several lines of evidence for a
312 selective sweep of an adaptive *C. robusta* allele introgressed into *C. intestinalis* at the hotspot and
313 identified a tandem repeat variation at the cytochrome P450 locus to be a promising candidate.

314 Introgression between highly divergent sea squirt genomes

315 Introgression between highly divergent lineages has been rarely reported, partly because there is a bias
316 against studying the end of the speciation continuum (Kulmuni et al. 2020). Indeed, the few cases that
317 documented introgression between divergent species consistently showed that it was rare and localized
318 to small genomic regions, suggesting that most introgression events were deleterious in the recipient
319 genome. Moreover, introgression occurred more often in regions depleted in conserved elements and
320 regions with high recombination rates, consistent with the idea that introgressed tracts escape the
321 effect of species barriers through recombination (Martin and Jiggins 2017). Examples include
322 drosophila flies (Turissini and Matute 2017), coccidioides fungi (Maxwell et al. 2019), nine-spined

323 sticklebacks (Yamasaki et al. 2020), sea snails (Stankowski et al. 2020) or aspen trees (Shang et al.
324 2020). In line with these previous findings, we found that gene flow was limited between the two
325 divergent sea squirt species, and that most introgressed tracts segregating within *C. intestinalis* were
326 short.

327 Based on coding sequences, previous work inferring the divergence history between *C.*
328 *robusta* and *C. intestinalis* found contrasting results. With sampling locations situated in the sympatric
329 and allopatric ranges of the two species, Roux et al. (2013) found evidence for introgression after
330 secondary contact. However, when they used only allopatric populations in a later work (Roux et al.
331 2016), and included the effect of linked selection by introducing within genome variations in effective
332 population size, they found unsupported evidence for ongoing gene flow. These differences illustrate
333 the effect of the sampling locations on the demographic inferences and demonstrate the importance of
334 geography to understand the complex history of divergence in non-indigenous species. Furthermore,
335 the two studies by Roux et al. differ in the set of models compared. Failing to account accurately for
336 genomic heterogeneity in gene flow or effective population size could result in falsely supporting a
337 wrong model (Roux et al. 2016).

338 Here, we tested whether the presence of many short and a few very long *C. robusta*
339 introgressed tracts in the genome of the sympatric *C. intestinalis* species could be explained by a
340 complex history of gene flow between the two species. Therefore, we fitted models that could include
341 genomic heterogeneities in effective population sizes and migration rates as well as periodic
342 connectivity between the two species. Despite a firm species boundary with about two-thirds of the
343 genome linked to species barriers, we found signals of past introgression (in the last ~30 Ky), far
344 preceding their contemporary contact in Europe. This is in line with the low rates of natural
345 hybridization between the two species (Bouchemousse, Liautard-Haag, et al. 2016). The pattern of
346 high differentiation we observed along the genomes also suggests highly polygenic barriers that
347 maintain the species boundaries between *C. robusta* and *C. intestinalis*. As the species diverged for

348 ~1.5 to 2 million years in strict isolation, they had time to accumulate many barriers in their genomes,
349 contributing to selection against introgression upon secondary contact.

350 These inferences were made excluding chromosome 5 to capture the prominent history
351 between the two species. When including this chromosome, and so the long introgressed tracts in the
352 introgression hotspot, we found evidence for a much more recent introgression event dated 200 years
353 ago. This estimate was then refined using a recombination clock and the introgressed tract length
354 distribution. We found that the contemporary introgression event may have occurred about 75 years
355 ago, consistent with the human-induced introduction of *C. robusta* in the English Channel (Nydam and
356 Harrison 2011; Bouchemousse, Bishop, et al. 2016).

357 Is there an adaptive breakthrough on chromosome 5?

358 In line with the studies mentioned above on divergent species, we observed limited introgression
359 between *C. robusta* and *C. intestinalis* in the sympatric range. On top of the many short introgressed
360 tracts (average length of 2.6 Kb) widespread in the *C. intestinalis* genome and segregating at a low
361 frequency, we observed a very localized introgression signal between 700 Kb and 1.5 Mb on
362 chromosome 5. This hotspot of introgression harbored very long introgression tracts (maximal length
363 of 156 Kb) that were more frequent than the baseline introgression level. This pattern contrasts with
364 the tract length distribution observed in a secondary contact between two divergent *Drosophila* fly
365 species that diverged 3 My ago (Turissini and Matute 2017). Introgression produced mostly small
366 tracts (1 to 2.5 Kb on average), but the longest tracts were only 7.5 to 10 Kb long, ten times smaller
367 than what was observed in the sea squirt hotspot. The situation in sea squirts resembles more to the
368 introgression pattern between two fungi species that diverged 5 My ago (Maxwell et al. 2019). Most
369 introgression tracts were 3 to 4 Kb long on average and segregated at low frequency, but there was a
370 long tail of longer tracts (maximal length of 100 Kb), some of them being found in high frequency
371 within species.

372 Adaptive introgressed alleles are expected to increase in frequency in the recipient population.
373 However, alleles might also increase in frequency simply due to allele surfing at the front wave of a
374 range expansion (Klopfstein et al. 2006). In our study, we only sampled populations in the English
375 Channel (Aber and Brest), but Le Moan et al. (2021) demonstrated that the introgression hotspot was
376 present in multiple localities (10 of 18) across the contact zone (Bay of Biscay, Iroise Sea and the
377 English Channel). The populations we sampled in Aber and Brest were among the most introgressed,
378 together with populations in the western UK coastline. However, there was no evidence for a wave of
379 introgression in line with geography: the distribution of introgressed tracts was a geographic mosaic,
380 likely due to human-mediated transportation (Le Moan et al. 2021).

381 Furthermore, the introgression of genomic tracts across a species barrier is highly random at
382 short time scales. Therefore, one expects a large variance in the tract length distribution under neutral
383 admixture (Sachdeva and Barton 2018). Observing long haplotypes at intermediate frequency could
384 thus be explained with purely neutral processes. Still, the singularity of such a region found in the
385 genome of sympatric *C. intestinalis* individuals seems difficult to explain without invoking some sort
386 of selection. We identified signals of selection based on haplotype variations in the flanking regions of
387 the most introgressed alleles (Sabeti et al. 2002; Staubach et al. 2012). Indeed, the introgression
388 hotspot is characterized by unusually long-range LD in the introgressed *C. intestinalis* population. The
389 genealogy at the hotspot shows that the haplotypes sampled in C. intestinalis cluster together with the
390 start-like clade of the *C. robusta* haplotypes. This indicates that a recent selective sweep occurred in
391 the *C. robusta* population, leading to the fixation of a beneficial allele, which then introgressed into the
392 sympatric *C. intestinalis* populations. This scenario was supported using an independent method based
393 on polarized SNPs (Setter et al. 2020; Szpiech et al. 2021).

394 Nevertheless, we cannot claim yet that the hotspot on chromosome 5 contains alleles that were
395 adaptively introgressed *sensu stricto*. Indeed, the introgression is not fixed in the studied *C.*
396 *intestinalis* population (maximal frequency of 0.31), nor in other distant localities of the contact zone

397 included in (Le Moan et al. 2021). Le Moan et al. suggested that the maintenance of polymorphism at
398 these alleles could be explained with some sort of balancing selection: if the introgressed tracts are
399 under overdominance or frequency-dependent selection, and suffer a fitness reduction when frequent
400 and homozygous in a foreign genetic background. Therefore, an incomplete sweep aligns with
401 balancing selection acting on the introgressed alleles (e.g., humans and neanderthals: Sams et al.
402 2016). In addition, this pattern is also expected if admixture is very recent, typically when it has been
403 human-mediated, as then allele replacement may still be ongoing in the recipient population. For
404 example, this may be the case in honeybees where a haplotype of European ancestry, implicated in
405 reproductive traits and foraging, was found at high frequency (but not fixed) in Africanized honeybees
406 (Nelson et al. 2017, confirmed in Calfee et al. 2020). Incomplete introgression at a single region has
407 also been documented in cotton bollworm, where an insecticide resistance allele at a cytochrome P450
408 gene increased in frequency after introducing an invasive congener carrying the adaptation (Valencia-
409 Montoya et al. 2020).

410 A usual suspect: cytochrome P450

411 In the middle of the introgression hotspot, we identified a region with high coverage that we could not
412 analyze using called genotypes (from 1,009,000 to 1,055,000 bp). Therefore, we examined the read
413 depth at candidate SNPs in this genomic region to identify further variants introgressing at a high
414 frequency. This analysis pinpointed 28 candidate SNPs, of which one in a non-coding region was at a
415 high frequency (0.85), but its overall low read depth calls for caution. The second most introgressed
416 SNPs (n=16) were located on the cytochrome P450 family 2 subfamily U gene, and all showed the
417 same introgression pattern with a frequency of 0.35. Strikingly, the *C. robusta* alleles had a read depth
418 pattern consistent with them being multi-copy (5 to 20 copies), while this was not the case for the *C.*
419 *intestinalis* alleles sampled in the non-introgressed individuals.

420 These candidate variants could potentially be involved in adaptation. Notably, the cytochrome
421 P450 gene is an exciting candidate. It belongs to a large gene class of oxidase enzymes responsible for

422 the biotransformation of small endogenous molecules, detoxifying exogenous compounds, and it is
423 involved in regulating the circadian rhythm. Cytochrome P450 family 2 is the largest and most diverse
424 CYP family in vertebrates, and the U and R subfamilies were present in the vertebrate ancestor
425 (Nelson 1998). A recent study experimentally showed that the candidate gene we identified here
426 (cytochrome P450 2U) is involved in the inflammatory response in *C. robusta* (Vizzini et al. 2021).
427 Although this phenotype indicates resistance toward toxic substances, future functional study of
428 potential fitness differences between the tandem repeat *C. robusta* allele and the single copy *C.*
429 *intestinalis* allele will be needed to determine what adaptive role these alleles play. Note, however, that
430 if the tandem-repeat variant provides adaptation to pollution in harbors, this would result in local
431 selection and explain the absence of fixation (the native alleles being fitter in wild habitats), as
432 discussed above.

433 At a larger phylogenetic scale, resistance genes were identified as gene families enriched in
434 adaptive introgressions (Moran et al. 2021). Notably, human-induced selection such as insecticide
435 exposure drives strong and rapid development of resistance. In that context, gene amplification of
436 detoxification enzymes is a crucial feature for adaptation as it increases the number of functional
437 enzymes and/or allows neofunctionalization of the new copies. There are many examples of such
438 processes involving cytochromes P450 in insects. Insecticide resistance is due to gene amplification
439 that produces over-expression of the cytochrome P450 gene in the aphid *Myzus persicae*
440 (neonicotinoids resistance, Puinean et al. 2010), *Drosophila melanogaster* (DDT resistance, Schmidt
441 et al. 2010), *Anopheles funestus* (pyrethroid resistance, Wondji et al. 2009), and *Anopheles coluzzii*
442 (ITN resistance, Main et al. 2018). Neonicotinoids resistance due to neofunctionalization of a
443 duplicated cytochrome P450 was demonstrated in the brown planthopper, *Nilaparvata lugens* (Zimmer
444 et al. 2018). Another example of high copy numbers of cytochrome P450 conferring insecticide
445 resistance was found in the moth *Spodoptera frugiperda* (Yainna et al. 2021). In contrast, resistance
446 against pyrethroid in the moth *Helicoverpa armigera* and introgressed *Helicoverpa zea* was due to a

447 chimeric cytochrome P450 gene resulting from recombination between two copies in tandem
448 (Valencia-Montoya et al. 2020).

449 Even though we are not yet at the step of functionally characterizing the cytochrome P450
450 candidate gene, we highlighted in this work the critical role of biological invasions for driving
451 adaptive introgression across species boundaries. Our work also illustrates that phased genomes offer
452 the opportunity to detect introgression signals between divergent species, even when they are rare and
453 localized in the genome. Genomically localized introgression breakthroughs are still an understudied
454 pattern that recent genomic surveys have only begun to unravel.

455 Materials and Methods

456 Sampling and whole-genome sequencing

457 Sixteen parent-offspring trios (six interspecific, six within *Ciona intestinalis* and four within *Ciona*
458 *robusta*) were generated by crossing wild-caught parents in the laboratory at Roscoff (**Table S1**). For
459 *C. intestinalis*, seven of the parents used were sampled in the marina of the Aber Wrac'h (Finistère,
460 France), and nine others in the marina of Moulin Blanc, Brest (Finistère, France). For *C. robusta*, the
461 ten parents used were also sampled in Moulin Blanc. The two parents and one randomly selected
462 descendant for each trio were fixed in absolute ethanol, and their whole genomic DNA was extracted
463 using a CTAB protocol. Five individuals were sampled in Banyuls-Sur-Mer (Méditerranée, France)
464 belonging to *Ciona roulei.* Based on crossing experiments and genetic analyses, the species status of
465 *C. roulei* has been repeatedly questioned (Nydam and Harrison 2010; Malfant et al. 2018; Le Moan et
466 al. 2021). In particular, recent genetic analyses clearly showed that *C. roulei* is a distinct lineage of *C.*
467 *intestinalis*, specific to the Mediterranean Sea (Le Moan et al. 2021). Therefore, we used these
468 individuals as a positive control for a non-introgressed population of *C. intestinalis*. For *C. roulei*
469 samples, genomic DNA was extracted using a Nucleospin Tissue kit (Macherey-Nagel). After quality
470 control, DNA extracts were sent to the LIGAN genomics platform (Lille, France) where whole-

471 genome sequencing libraries were prepared separately for each of the 48 individuals, and were
472 sequenced on an Illumina Hi-Seq 2000 instrument using 100 bp PE reads. Three parents that were
473 poorly sequenced (ad2, ad18 and ad31; **Table S1**) were excluded from analyses.

474 Furthermore, four *Ciona edwardsi* individuals were sampled in Banyuls-Sur-Mer. *C. edwardsi*
475 is reproductively isolated from the other taxa included in this study, and it was used as an outgroup
476 (Malfant et al. 2018). These individuals were fixed in RNAlater, and their DNA was extracted using a
477 Nucleospin Tissue kit (Macherey-Nagel). Libraries were prepared separately for each of the four
478 individuals, and were sequenced on an Illumina Hi-Seq 4000 instrument using 150 bp PE reads at
479 FASTERIS (Plan-les-Ouates, Switzerland).

480 Genotyping and haplotyping pipeline

481 We followed the GATK best practice pipeline (Van der Auwera et al. 2013) including haplotype
482 phasing-by-transmission, as applied in Duranton et al. (2018). All scripts used in the pipeline are
483 available in the **Supplementary Scripts**. We generated seven different datasets with various levels of
484 filtering, and with or without haplome phasing, that are described in the **Supplementary Data**.

485 All analyses were made using the newly available *C. robusta* assembly as the reference
486 genome (GCA_009617815.1; Satou et al. 2019). As a cautionary note, analyses in Le Moan et al.
487 (2021) were made using the previous *C. robusta* reference genome published in 2011
488 (GCA_000224145.1), therefore coordinates do not correspond between the two studies. Reads were
489 aligned to the *C. robusta* reference genome using BWA-mem v0.7.5a (Li and Durbin 2009), and
490 duplicates were marked using Picard v1.119. The individual bam files of the introgression hotspot
491 were used as dataset **#7**. The mean read depth was 21x across all samples (**Table S1**).

492 A series of steps were then performed using GATK v3.4-0 (McKenna et al. 2010), including:
493 *i*) local realignment around indels, *ii*) individual variant calling in gVCF format using the
494 HaplotypeCaller (options: dontUseSoftClippedBases, heterozygosity=0.01, minimum base quality
495 score=30), *iii*) joint genotyping using GenotypeGVCFs (heterozygosity=0.01), *iv*) genotype

496 refinement based on family priors. Hard-filtering was then applied on the SNPs and indels to produce
497 a database of high-confidence variants. The database was then used to recalibrate variant quality
498 scores with the VQSR algorithm. After recalibration, a second round of genotype refinement based on
499 family priors was applied.

500 We then introduced a step of genotype verification (and correction where required) based on
501 the individual variant allele fraction (VAF) at each site, i.e., the ratio of the alternate allele depth to the
502 total (alternate+reference) depth. A distribution across sites was plotted for the three possible
503 genotypes (homozygous reference: 0/0, heterozygous: 0/1, homozygous alternate: 1/1). While the
504 distributions for the homozygous genotypes were shaped as expected (i.e. 99% of the sites had a VAF
505 < 0.1 for 0/0 and VAF > 0.9 for 1/1), the distribution of heterozygous genotypes was normally
506 distributed around VAF=0.5, but showed additional peaks near 0 (and near 1 to a lesser extent).
507 Therefore, we corrected the miscalled 0/1 genotypes to 0/0 when the variant allele depth was below
508 the 99th quantile of the 0/0 distribution and to 1/1 when it was above the 1th quantile of the 1/1
509 distribution. In addition, heterozygous genotypes with a VAF < ⅓ or > ⅔ were assigned as missing
510 data (excluding the ones we corrected near VAF=0 or 1). We also considered as missing data the
511 genotypes with a total depth below ten reads or above the 99th quantile of the depth distribution (to
512 exclude repeated regions). Finally, low-quality variants were excluded from the VCF (QUAL<30), and
513 we applied a stringent filter on individual genotype quality (GQ<30). Different missing data thresholds
514 were then applied to produce datasets **#2** (five missing genotypes), **#5** (no missing genotypes allowed)
515 and **#6** (three missing genotypes).

516 Phased genomes were obtained using the tool PhaseByTransmission of GATK v3.4-0. All trios
517 were phased given parents and offspring genotype likelihoods, setting a *de novo* mutation prior to 1e-
518 8. Only sites where Mendelian transmission could be determined unambiguously were phased. The
519 non-missing phased SNPs were then used as a reference panel for BEAGLE v4.0 (Browning and
520 Browning 2007). BEAGLE was run without imputing genotypes (impute=false) on the filtered VCF,

521 with all variants being unphased. The parent-offspring relationships in the reference panel were
522 specified to inform phasing-by-transmission with BEAGLE, except for the five *C. roulei* samples,
523 which were not included in a trio and were statistically phased. Datasets **#1**, **#3** and **#4** are based on
524 this phased VCF.

525 A genomic region with high coverage failed to be genotyped in the introgression hotspot
526 (defined between 700 Kb and 1.5 Mb). This region was set as the "missing data region" and defined
527 from 1,009,000 to 1,055,000 bp.

528 Analyses of population structure

529 We used a Principal Component Analysis (PCA) to assess the partition of genetic variation in our
530 sample of 45 individuals (i.e., all individuals except the three poorly sequenced parents, and the *C.*
531 *edwardsi* individuals). SNPs were LD-pruned with PLINK v1.9 (Purcell et al. 2007) using a window
532 size (WD) of 20 SNPs, a window step size (CT) of 5 SNPs and a linkage threshold (r^2) of 0.1. PLINK
533 was then used to run a PCA on the unlinked SNPs. We recorded the amount of genotypic variance
534 explained by each principal component (PC) and the SNP weights on each PC. Only the first two PCs
535 were relevant to visualize population structure and were plotted using the R package tidyverse.

536 We used VCFtools v0.1.15 (Danecek et al. 2011) on all SNPs to calculate the per-site
537 nucleotide diversity (site-pi) in each population and the per-site F_{ST} (weir-fst-pop, Weir and
538 Cockerham 1984) between populations. We then calculated the average and maximum of these
539 statistics for each chromosome in non-overlapping windows of 10 Kb. Windows with less than 10
540 SNPs were excluded. The linkage disequilibrium on chromosome 5 (where an introgression hotspot
541 was detected) in the *C. intestinalis* individuals was estimated with the function "hap-r2" of VCFtools.
542 It was based on the calculation of the r^2 among all fixed SNPs (phased) between *C. robusta* and *C.*
543 *roulei*.

544 Detection of introgression with summary statistics

545 To evaluate the extent of genome-wide admixture, we computed the D-statistic (Green et al. 2010;
546 Patterson et al. 2012) from a polarized set of SNPs using the outgroup species, *C. edwardsi*. The
547 following topology was applied: (((P1 = *C. roulei* ; P2 = *C. intestinalis*) ; P3 = *C. robusta*) ; O = *C.*
548 *edwardsi*). Therefore, a positive value of D indicates an excess of ABBA sites, and so an excess of
549 shared ancestry of *C. robusta* with *C. intestinalis* over that shared with *C. roulei*. We also estimated the
550 fraction of the genome introgressed with the *fd* statistic (Martin et al. 2015), calculated in non-
551 overlapping windows of 100 SNPs.

552 Detection of introgression with local ancestry inference

553 We used Chromopainter (available in fineSTRUCTURE v2.0.7) to perform local ancestry inference
554 based on the phased dataset. *C. intestinalis* was considered as the recipient population, while *C.*
555 *robusta* and *C. roulei* (the latter being a non-introgressed population of *C. intestinalis*) were the donor
556 populations. We used ten iterations of the expectation-maximization algorithm to estimate the
557 probability of each position along each *C. intestinalis* haplotype to come from *C. robusta* or *C. roulei*.
558 We then determined the boundaries of each ancestry tract. A given position was considered originating
559 from *C. robusta* if this probability was >0.95. To define the tracts, an extension from this focal position
560 was then made as long as this probability was above 0.5 at the surrounding positions (Duranton et al.
561 2018).

562 Various statistics were then calculated focusing on the introgressed tracts originating from *C.*
563 *robusta* (i.e. those found in *C. intestinalis* haplotypes, but with a *C. robusta* ancestry): *i*) the *C. robusta*
564 ancestry fraction per individual, *ii*) the tract length, and *iii*) the frequency of the alleles lying on the
565 tracts. No filter on the minimal tract length was applied, and missing data were not allowed for the
566 allele frequency calculation.

567 We performed additional analyses on the coding sequences (CDS). They were obtained by
568 extracting the biallelic SNPs from the phased VCF. Then, the VCF was converted into a fasta file, and

569 exons were extracted with bedtools v2.25.0 based on the annotation file (HT.Gene.gff3) of the
570 reference genome. The CDS were classified as introgressed or not using the bounds inferred from
571 Chromopainter. The following statistics were calculated for the CDS: *i*) the pairwise nucleotide
572 diversity (π, Tajima 1983), *ii*) the raw divergence between *C. robusta* and *C. intestinalis* (d_{XY}, Nei and
573 Li 1979), and *iii*) the G_{min} measured as minimum(d_{XY})/average(d_{XY}) (Geneva et al. 2015).

574 Testing for selection

575 Selection for an adaptive variant is expected to reduce haplotype variation in flanking regions,
576 producing unusually long haplotypes (Sabeti et al. 2002). To capture such a signal, we measured the
577 extended haplotype homozygosity (EHH) score from the phased dataset using SelScan v2.0.0 (Szpiech
578 2021). Target SNPs were identified as the *C. robusta* alleles with the highest frequency to the left
579 (959,519 bp) and right (1,061,854 bp) of the "missing data region" on chromosome 5. The maximum
580 extension from the target SNP for a single EHH computation was 100 Kb. Then, we calculated with
581 SelScan the (absolute) integrated haplotype score (iHS). Values were normalized using the norm
582 v1.3.0 utility with 100 frequency bins over 50-Kb non-overlapping windows. Finally, we estimated the
583 proportion of SNPs in each window associated with extreme iHS values (iHS>3, which refers to the
584 99th quantile of the iHS distribution).

585 We also tested for the footprint of selective sweeps using SweepFinder v2.0 (DeGiorgio et al.
586 2016) and adaptive introgression using VolcanoFinder v1.0 (Setter et al. 2020). These methods are
587 based on polarized SNPs (using the outgroup species *C. edwardsi*) and do not use phase information.
588 Chromosomes were scanned with the two methods, and a log-ratio test for selection was performed at
589 test sites spaced by 1Kb.

590 Finally, SplitsTree4 V4.17.0 (Huson and Bryant 2006) was used on the phased dataset to
591 produce neighbor-joining trees from 50-Kb windows framing the "missing data region" on
592 chromosome 5.

593 Analyses of copy number variation

594 To overcome the absence of genotyping in the "missing data region" (due to our filtering of repeated
595 regions), we analyzed the read depth of the variants directly from the unfiltered bam files. Counts of
596 the reference and alternate alleles were collected with GATK (CollectAllelicCounts) from the bam
597 files, excluding duplicate reads and positions with a base quality (BQ) < 20. Candidate SNPs were
598 defined based on their variant allele fraction (VAF = alternate read depth / total read depth). The
599 following criteria were applied to identify variants differentiated between *C. robusta* and *C. roulei* (the
600 latter is used as a non-introgressed *C. intestinalis* population), and introgressed into *C. intestinalis*:
601 VAF <= 50% in *C. intestinalis*, VAF >= 85% (or 90%) in *C. roulei* and VAF <= 15% (or 10%) in *C.*
602 *robusta*. The copy number at each candidate SNP was then calculated as its allele read depth
603 normalized by the per-site read depth averaged across all sites (excluding sites with less than ten
604 reads) for each individual. Variants were annotated using the HT.Gene.gff3 file of the reference
605 genome.

606 Demographic inferences

607 We reconstructed the divergence history of *C. robusta* and *C. intestinalis* from the folded joint site
608 frequency spectrum (jSFS) using moments (Jouganous et al. 2017). No missing data was allowed, and
609 the SNPs were LD-pruned with PLINK v1.9 using a window size (WD) of 10 SNPs, a window step
610 size (CT) of 10 SNPs and a linkage threshold (r^2) of 0.5. We defined five demographic scenarios,
611 following (Fraïsse et al. 2018): SI = strict isolation, IM = isolation with continuous migration, SC =
612 secondary contact, AM = ancient migration, PER = periodic connectivity with both an ancient and a
613 current period of gene flow. Different versions of these scenarios were tested, following (Fraïsse et al.
614 2021): bbN = genomic heterogeneity of the effective population sizes (to capture the effect of
615 background selection), bbM = genomic heterogeneity of the effective migration rates (to capture the
616 effect of interspecies barriers to gene flow), 2N2M = combining both types of heterogeneities, "" = no
617 heterogeneities. Parameters were as follows: T = times in years (assuming two generations per year in

European waters), Ne = effective population sizes in numbers of individuals, m = migration rates (independently estimated in both directions), %Barriers = fraction of the genome experiencing null migration (i.e. species barriers and their associated loci), $\%Ne_{reduced}$ = fraction of the genome experiencing reduced Ne due to background selection, HRF = factor by which Ne is reduced. See **Tables S3** and **S4** for details. The scripts used to define the demographic models and run the inferences are available in the **Supplementary Scripts**.

Each demographic model was then fitted to the observed jSFS, with singletons masked. We ran five independent runs from randomized starting parameter values for each model. Likelihood optimization was performed using a "dual annealing" algorithm (optimize_dual_anneal). It consists of a series of global optimizations, each followed by a local optimization ("L-BFGS-B" method). Settings of the global optimizations were as follows: maximum number of search iterations = 100, initial temperature = 50, acceptance parameter = 1, and visit parameter = 1.01. The maximum number of search iterations for the local optimization was set to 100. Model comparisons were made using the Akaike information criterion (AIC), calculated as $2*k$ - 2*ML, where k is the number of parameters in the model, and ML its maximum log-likelihood value across the five runs.

Data Availability

Sequence reads have been deposited in NCBI Sequence Read Archive (SRA) under the accession number PRJNA813009. Supplementary Data is available from Zenodo: XXX. Supplementary Figures, Tables and Scripts can be found in the Supporting Information.

Acknowledgments

The authors are grateful to the divers of the Marine Operations department (*Service Mer & Observation*) at the Roscoff Biological Station for the *Ciona* sampling in Brittany, and to Marine Malfant, Sebastien Darras and divers of the laboratory Arago in Banyuls-Sur-Mer for providing the

Ciona edwardsi and *C. roulei* samples, and Charlotte Roby for DNA extractions. The authors are very thankful to Jerome Coudret and Sarah Bouchemousse for their help for carrying the laboratory crosses at Roscoff. We thank Véronique Dhennin from the LIGAN genomics platform (Lille, France), and Nicolas González from the FASTERIS platform (Plan-les-Ouates, Switzerland). This work benefited from the Montpellier Bioinformatics Biodiversity platform supported by the LabEx CeMEB, an ANR ”Investissements d’avenir" program (ANR-10-LABX-04-01). This work benefited from funding of the French National Research Agency (ANR) with regards the ANR Project HYSEA (no. ANR-12-BSV7-0011). It also benefited from the MarEEE project funded through the French National Research Agency (ANR) under the “Investissements d’Avenir” programme with the reference ANR-16-IDEX-0006 (i-site MUSE). The funders had no role in study design, data collection and analysis, decision to publish, or preparation of the manuscript.

References

Bouchemousse S, Bishop JDD, Viard F. 2016. Contrasting global genetic patterns in two biologically similar, widespread and invasive Ciona species (Tunicata, Ascidiacea). *Sci. Rep.* 6:24875.

Bouchemousse S, Lévêque L, Dubois G, Viard F. 2016. Co-occurrence and reproductive synchrony do not ensure hybridization between an alien tunicate and its interfertile native congener. *Evol. Ecol.* 30:69–87.

Bouchemousse S, Lévêque L, Viard F. 2017. Do settlement dynamics influence competitive interactions between an alien tunicate and its native congener? *Ecol. Evol.* 7:200–213.

Bouchemousse S, Liautard-Haag C, Bierne N, Viard F. 2016. Distinguishing contemporary hybridization from past introgression with postgenomic ancestry-informative SNPs in strongly differentiated Ciona species. *Mol. Ecol.* 25:5527–5542.

Browning SR, Browning BL. 2007. Rapid and accurate haplotype phasing and missing-data inference for whole-genome association studies by use of localized haplotype clustering. *Am. J. Hum. Genet.* 81:1084–1097.

Calfee E, Agra MN, Palacio MA, Ramírez SR, Coop G. 2020. Selection and hybridization shaped the rapid spread of African honey bee ancestry in the Americas. *PLoS Genet.* 16:e1009038.

Danecek P, Auton A, Abecasis G, Albers CA, Banks E, DePristo MA, Handsaker RE, Lunter G, Marth GT, Sherry ST, et al. 2011. The variant call format and VCFtools. *Bioinformatics* 27:2156–2158.

DeGiorgio M, Huber CD, Hubisz MJ, Hellmann I, Nielsen R. 2016. SweepFinder2: increased sensitivity, robustness and flexibility. *Bioinformatics* 32:1895–1897.

Duranton M, Allal F, Fraïsse C, Bierne N, Bonhomme F, Gagnaire P-A. 2018. The origin and remolding of genomic islands of differentiation in the European sea bass. *Nature Comm.* 9:2518.

Fraïsse C, Popovic I, Mazoyer C, Spataro B, Delmotte S, Romiguier J, Loire É, Simon A, Galtier N, Duret L, et al. 2021. DILS: Demographic inferences with linked selection by using ABC. *Mol. Ecol. Resour.* 21:2629–2644.

Fraïsse C, Roux C, Gagnaire P-A, Romiguier J, Faivre N, Welch JJ, Bierne N. 2018. The divergence history of European blue mussel species reconstructed from Approximate Bayesian Computation: the effects of sequencing techniques and sampling strategies. *PeerJ* 6:e5198.

Geneva AJ, Muirhead CA, Kingan SB, Garrigan D. 2015. A New Method to Scan Genomes for Introgression in a Secondary Contact Model. *PLoS One* 10:e0118621.

Green RE, Krause J, Briggs AW, Maricic T, Stenzel U, Kircher M, Patterson N, Li H, Zhai W, Fritz MH-Y, et al. 2010. A draft sequence of the Neandertal genome. *Science* 328:710–722.

Hudson J, Viard F, Roby C, Rius M. 2016. Anthropogenic transport of species across native ranges:

unpredictable genetic and evolutionary consequences. *Biol. Lett.* 12:20160620.

Huson DH, Bryant D. 2006. Application of phylogenetic networks in evolutionary studies. *Mol. Biol. Evol.* 23:254–267.

Jouganous J, Long W, Ragsdale AP, Gravel S. 2017. Inferring the Joint Demographic History of Multiple Populations: Beyond the Diffusion Approximation. *Genetics* 206:1549–1567.

Kaback DB. 1996. Chromosome-size dependent control of meiotic recombination in humans. *Nat. Genet.* 13:20–21.

Klopfstein S, Currat M, Excoffier L. 2006. The fate of mutations surfing on the wave of a range expansion. *Mol. Biol. Evol.* 23:482–490.

Kulmuni J, Butlin RK, Lucek K, Savolainen V, Westram AM. 2020. Towards the completion of speciation: the evolution of reproductive isolation beyond the first barriers. *Philos. Trans. R. Soc. Lond. B Biol. Sci.* 375:20190528.

Le Moan A, Roby C, Fraïsse C, Daguin-Thiébaut C, Bierne N, Viard F. 2021. An introgression breakthrough left by an anthropogenic contact between two ascidians. *Mol. Ecol.* 30:6718–6732.

Li H, Durbin R. 2009. Fast and accurate short read alignment with Burrows-Wheeler transform. *Bioinformatics* 25:1754–1760.

Main BJ, Everitt A, Cornel AJ, Hormozdiari F, Lanzaro GC. 2018. Genetic variation associated with increased insecticide resistance in the malaria mosquito, Anopheles coluzzii. *Parasit. Vectors* 11:225.

Malfant M, Darras S, Viard F. 2018. Coupling molecular data and experimental crosses sheds light about species delineation: a case study with the genus Ciona. *Sci. Rep.* 8:1480.

706 Martin SH, Davey JW, Jiggins CD. 2015. Evaluating the Use of ABBA–BABA Statistics to Locate
707 Introgressed Loci. *Mol. Biol. Evol.* 32:244–257.

708 Martin SH, Jiggins CD. 2017. Interpreting the genomic landscape of introgression. *Curr. Opin. Genet.*
709 *Dev.* 47:69–74.

710 Maxwell CS, Mattox K, Turissini DA, Teixeira MM, Barker BM, Matute DR. 2019. Gene exchange
711 between two divergent species of the fungal human pathogen, Coccidioides. *Evolution* 73:42–58.

712 McFarlane SE, Pemberton JM. 2019. Detecting the True Extent of Introgression during Anthropogenic
713 Hybridization. *Trends Ecol. Evol.* 34:315–326.

714 McKenna A, Hanna M, Banks E, Sivachenko A, Cibulskis K, Kernytsky A, Garimella K, Altshuler D,
715 Gabriel S, Daly M, et al. 2010. The Genome Analysis Toolkit: a MapReduce framework for
716 analyzing next-generation DNA sequencing data. *Genome Res.* 20:1297–1303.

717 Moran BM, Payne C, Langdon Q, Powell DL, Brandvain Y, Schumer M. 2021. The genomic
718 consequences of hybridization. *Elife* 10:e69016.

719 Nei M, Li WH. 1979. Mathematical model for studying genetic variation in terms of restriction
720 endonucleases. *Proc. Natl. Acad. Sci. U. S. A.* 76:5269–5273.

721 Nelson DR. 1998. Metazoan cytochrome P450 evolution. *Comp. Biochem. Physiol. C Pharmacol.*
722 *Toxicol. Endocrinol.* 121:15–22.

723 Nelson RM, Wallberg A, Simões ZLP, Lawson DJ, Webster MT. 2017. Genomewide analysis of
724 admixture and adaptation in the Africanized honeybee. *Mol. Ecol.* 26:3603–3617.

725 Noé L, Kucherov G. 2005. YASS: enhancing the sensitivity of DNA similarity search. *Nucleic Acids*
726 *Res.* 33:W540–W543.

North HL, McGaughran A, Jiggins CD. 2021. Insights into invasive species from whole-genome resequencing. *Mol. Ecol.* 30:6289–6308.

Nydam ML, Harrison RG. 2010. Polymorphism and divergence within the ascidian genus Ciona. *Mol. Phylogenet. Evol.* 56:718–726.

Nydam ML, Harrison RG. 2011. Introgression despite substantial divergence in a broadcast spawning marine invertebrate. *Evolution* 65:429–442.

Purcell S, Neale B, Todd-Brown K, Thomas L, Ferreira MAR, Bender D, Maller J, Sklar P, de Bakker PIW, Daly MJ, Sham PC. 2007. PLINK: a toolset for whole-genome association and population-based linkage analysis. *Am. J. Hum. Genet.* 81.

Ottenburghs J. 2021. The genic view of hybridization in the Anthropocene. *Evol. Appl.* 14:2342–2360.

Patterson N, Moorjani P, Luo Y, Mallick S, Rohland N, Zhan Y, Genschoreck T, Webster T, Reich D. 2012. Ancient admixture in human history. *Genetics* 192:1065–1093.

Puinean AM, Foster SP, Oliphant L, Denholm I, Field LM, Millar NS, Williamson MS, Bass C. 2010. Amplification of a cytochrome P450 gene is associated with resistance to neonicotinoid insecticides in the aphid Myzus persicae. *PLoS Genet.* 6:e1000999.

Racimo F, Sankararaman S, Nielsen R, Huerta-Sánchez E. 2015. Evidence for archaic adaptive introgression in humans. *Nat. Rev. Genet.* 16:359–371.

Ravinet M, Yoshida K, Shigenobu S, Toyoda A, Fujiyama A, Kitano J. 2018. The genomic landscape at a late stage of stickleback speciation: High genomic divergence interspersed by small localized regions of introgression. *PLoS Genet.* 14:e1007358.

Robinson JT, Thorvaldsdóttir H, Winckler W, Guttman M, Lander ES, Getz G, Mesirov JP. 2011. Integrative genomics viewer. *Nat. Biotechnol.* 29:24–26.

Roux C, Fraïsse C, Romiguier J, Anciaux Y, Galtier N, Bierne N. 2016. Shedding Light on the Grey Zone of Speciation along a Continuum of Genomic Divergence. *PLoS Biol.* 14:e2000234.

Roux C, Tsagkogeorga G, Bierne N, Galtier N. 2013. Crossing the species barrier: genomic hotspots of introgression between two highly divergent Ciona intestinalis species. *Mol. Biol. Evol.* 30:1574–1587.

Sabeti PC, Reich DE, Higgins JM, Levine HZP, Richter DJ, Schaffner SF, Gabriel SB, Platko JV, Patterson NJ, McDonald GJ, et al. 2002. Detecting recent positive selection in the human genome from haplotype structure. *Nature* 419:832–837.

Sachdeva H, Barton NH. 2018. Introgression of a Block of Genome Under Infinitesimal Selection. *Genetics* 209:1279–1303.

Sams AJ, Dumaine A, Nédélec Y, Yotova V, Alfieri C, Tanner JE, Messer PW, Barreiro LB. 2016. Adaptively introgressed Neandertal haplotype at the OAS locus functionally impacts innate immune responses in humans. *Genome Biol.* 17:246.

Satou Y, Nakmura R, Deli Y, Yoshida R, Hamada M, Fujie M, Hisata K, Takeda H, Satoh N. 2019. A nearly-complete genome of Ciona intestinalis type A (C. robusta) reveals the contribution of inversion to chromosomal evolution in the genus Ciona. *Genome Biol. Evol.* 11:3144–3157.

Schmidt JM, Good RT, Appleton B, Sherrard J, Raymant GC, Bogwitz MR, Martin J, Daborn PJ, Goddard ME, Batterham P, et al. 2010. Copy number variation and transposable elements feature in recent, ongoing adaptation at the Cyp6g1 locus. *PLoS Genet.* 6:e1000998.

Setter D, Mousset S, Cheng X, Nielsen R, DeGiorgio M, Hermisson J. 2020. VolcanoFinder: Genomic scans for adaptive introgression. *PLoS Genet.* 16:e1008867.

Shang H, Hess J, Pickup M, Field DL, Ingvarsson PK, Liu J, Lexer C. 2020. Evolution of strong

771 reproductive isolation in plants: broad-scale patterns and lessons from a perennial model group.
772 *Philos. Trans. R. Soc. Lond. B Biol. Sci.* 375:20190544.

773 Shenkar N, Swalla BJ. 2011. Global diversity of Ascidiacea. *PLoS One* 6:e20657.

774 Shoguchi E, Kawashima T, Satou Y, Hamaguchi M, Sin-I T, Kohara Y, Putnam N, Rokhsar DS, Satoh
775 N. 2006. Chromosomal mapping of 170 BAC clones in the ascidian Ciona intestinalis. *Genome*
776 *Res.* 16:297–303.

777 Simon A, Arbiol C, Nielsen EE, Couteau J, Sussarellu R, Burgeot T, Bernard I, Coolen JWP, Lamy J-
778 B, Robert S, et al. 2020. Replicated anthropogenic hybridisations reveal parallel patterns of
779 admixture in marine mussels. *Evol. Appl.* 13:575–599.

780 Stachowicz JJ, Terwin JR, Whitlatch RB, Osman RW. 2002. Linking climate change and biological
781 invasions: Ocean warming facilitates nonindigenous species invasions. *Proc. Natl. Acad. Sci. U.*
782 *S. A.* 99:15497–15500.

783 Stankowski S, Westram AM, Zagrodzka ZB, Eyres I, Broquet T, Johannesson K, Butlin RK. 2020. The
784 evolution of strong reproductive isolation between sympatric intertidal snails. *Philos. Trans. R.*
785 *Soc. Lond. B Biol. Sci.* 375:20190545.

786 Staubach F, Lorenc A, Messer PW, Tang K, Petrov DA, Tautz D. 2012. Genome patterns of selection
787 and introgression of haplotypes in natural populations of the house mouse (Mus musculus). *PLoS*
788 *Genet.* 8:e1002891.

789 Szpiech ZA. 2021. Selscan 2.0: scanning for sweeps in unphased data. *biorxiv*. 2021.10.22.465497.

790 Tajima F. 1983. Evolutionary relationship of DNA sequences in finite populations. *Genetics* 105:437–
791 460.

792 Turissini DA, Matute DR. 2017. Fine scale mapping of genomic introgressions within the Drosophila

793 yakuba clade. *PLoS Genet.* 13:e1006971.

794 Valencia-Montoya WA, Elfekih S, North HL, Meier JI, Warren IA, Tay WT, Gordon KHJ, Specht A,
795 Paula-Moraes SV, Rane R, et al. 2020. Adaptive Introgression across Semipermeable Species
796 Boundaries between Local Helicoverpa zea and Invasive Helicoverpa armigera Moths. *Mol. Biol.*
797 *Evol.* 37:2568–2583.

798 Van der Auwera GA, Carneiro MO, Hartl C, Poplin R, Del Angel G, Levy-Moonshine A, Jordan T,
799 Shakir K, Roazen D, Thibault J, et al. 2013. From FastQ data to high confidence variant calls: the
800 Genome Analysis Toolkit best practices pipeline. *Curr. Protoc. Bioinformatics* 43:11.10.1–
801 11.10.33.

802 Viard F, Riginos C, Bierne N. 2020. Anthropogenic hybridization at sea: three evolutionary questions
803 relevant to invasive species management. *Philos. Trans. R. Soc. Lond. B Biol. Sci.* 375:20190547.

804 Vizzini A, Bonura A, La Paglia L, Fiannaca A, La Rosa M, Urso A, Mauro M, Vazzana M, Arizza V.
805 2021. Transcriptomic Analyses Reveal 2 and 4 Family Members of Cytochromes P450 (CYP)
806 Involved in LPS Inflammatory Response in Pharynx of *Ciona robusta*. *Int. J. Mol. Sci.* 22:11141.

807 Weir BS, Cockerham CC. 1984. Estimating f-statistics for the analysis of population structure.
808 *Evolution* 38:1358–1370.

809 Wondji CS, Irving H, Morgan J, Lobo NF, Collins FH, Hunt RH, Coetzee M, Hemingway J, Ranson
810 H. 2009. Two duplicated P450 genes are associated with pyrethroid resistance in Anopheles
811 funestus, a major malaria vector. *Genome Research* 19:452–459.

812 Yainna S, Nègre N, Silvie PJ, Brévault T, Tay WT, Gordon K, dAlençon E, Walsh T, Nam K. 2021.
813 Geographic Monitoring of Insecticide Resistance Mutations in Native and Invasive Populations
814 of the Fall Armyworm. *Insects* 12:468.

Yamasaki YY, Kakioka R, Takahashi H, Toyoda A, Nagano AJ, Machida Y, Møller PR, Kitano J. 2020. Genome-wide patterns of divergence and introgression after secondary contact between Pungitius sticklebacks. *Philos. Trans. R. Soc. Lond., B, Biol. Sci.* 375:20190548.

Zhan A, Briski E, Bock DG, Ghabooli S, MacIsaac HJ. 2015. Ascidians as models for studying invasion success. *Mar. Biol.* 162:2449–2470.

Zimmer CT, Garrood WT, Singh KS, Randall E, Lueke B, Gutbrod O, Matthiesen S, Kohler M, Nauen R, Davies TGE, et al. 2018. Neofunctionalization of Duplicated P450 Genes Drives the Evolution of Insecticide Resistance in the Brown Planthopper. *Curr. Biol.* 28:268–274.e5.

823 **Figure 1** Genetic population structure. **A.** Geographical location of the samples in the English Channel and
824 Iroise Sea (*C. robusta* and *C. intestinalis*) and the Mediterranean Sea (*C. roulei*). Numbers in brackets refer to the
825 sample size of each population. "Lab F1s" indicates the intraspecific and interspecific offspring produced in the
826 laboratory. Further information on samples is provided in **Table S1**. The color code (*C. robusta* in red, *C.*
827 *intestinalis* in blue and *C. roulei* in green) is used throughout the manuscript. **B.** Principal Component Analysis
828 of 45 individuals genotyped at 194,742 unlinked SNPs (pruning threshold: $r^2 > 0.1$). Numbers in brackets refer to
829 the proportion of variance explained by each axis. The F1s were considered as supplementary individuals in the
830 PCA, and three poorly sequenced parents were removed from the analysis (see **Table S1**). **C.** SNP weights to the
831 first axis of the PCA (after removing the SNPs contributing less than the 75th quantile of the weight
832 distribution). The introgression hotspot on chromosome 5 is highlighted with an arrow. Dataset **#1** was used.

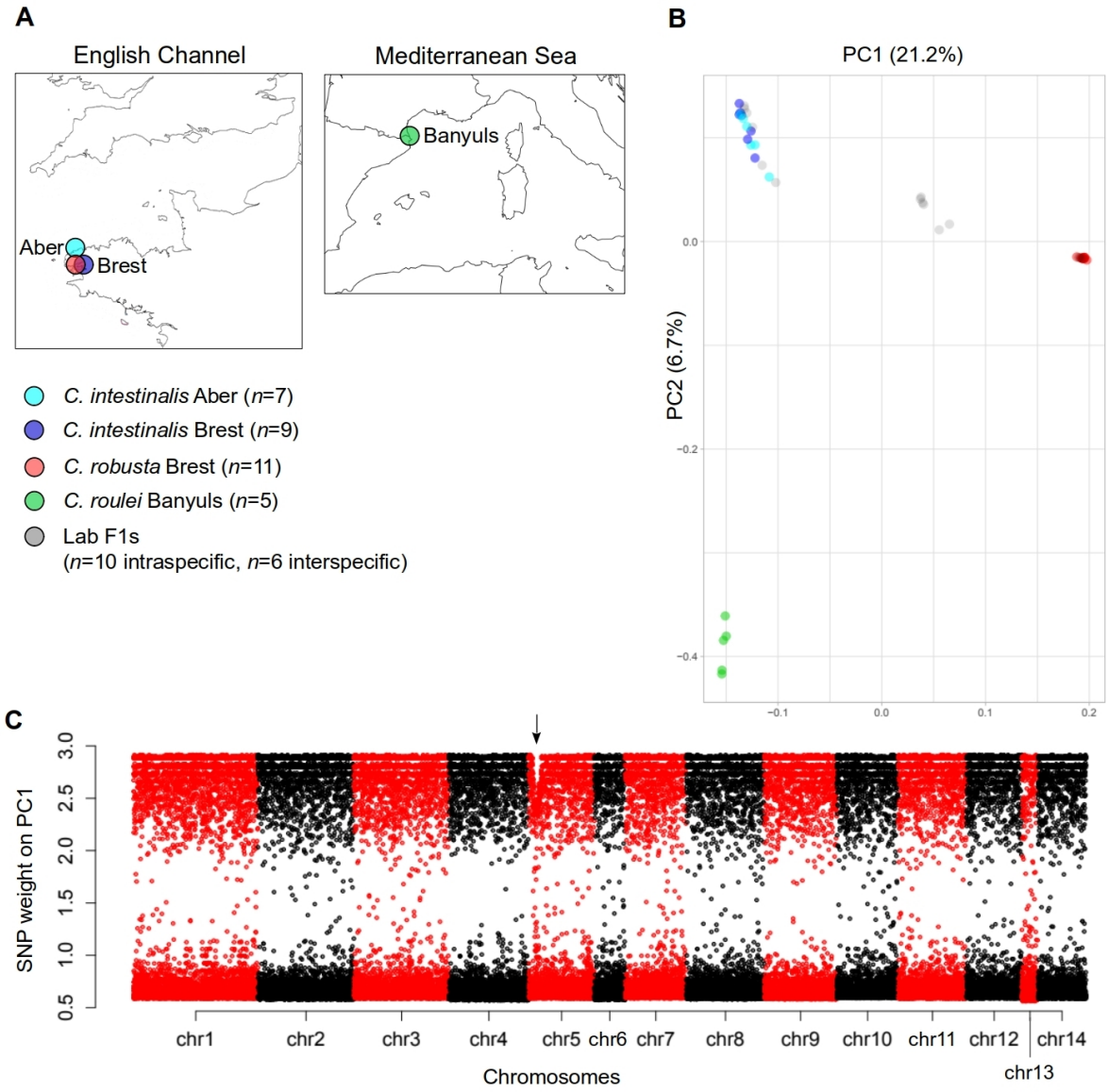

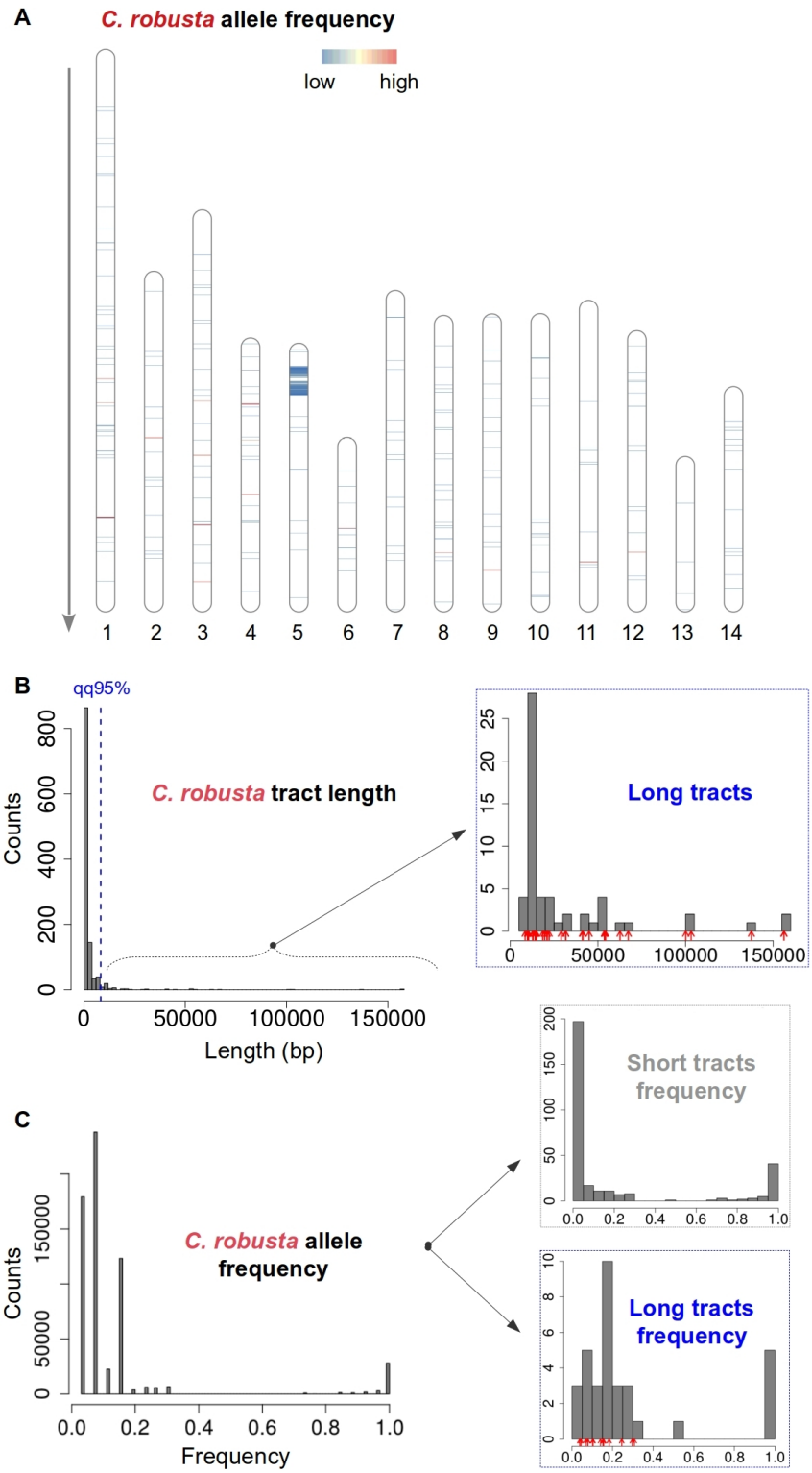

Figure 2 Local ancestry patterns of the *C. intestinalis* genomes sampled in the English Channel and Iroise Sea using 640,044 phased SNPs. *C. robusta* and *C. roulei* were used as the donor populations. **A.** Physical mapping across the 14 chromosomes of the frequency of the *C. robusta* tracts introgressed into *C. intestinalis*. The color gradient (blue to yellow to red) follows the gradient in allele frequency from low to high; regions in white correspond to null introgression. The direction of the arrow indicates the coordinate direction from top (start) to bottom (end). The R package RIdeograms was used for the plotting. **B.** Length distribution of the *C. robusta* introgressed tracts (*n*=1,143 tracts). The maximum tract length is 156 Kb, the average is 2.6 Kb, and the median is 0.38 Kb. A blue dashed line depicts the 95th quantile of the length distribution (8.3 Kb), and it was used as a threshold to delineate long tracts. A total of 38 of 57 long tracts were detected on chromosome 5 (red arrows). **C.** Allele frequency of the SNPs lying on the *C. robusta* introgressed tracts (*n*=621,249 variants). The maximum frequency is 1, the average is 0.14, and the median is 0.08. On the right, the frequency of variants lying on short tracts (upper panel) or long tracts (lower panel) is depicted. Red arrows indicate the tracts on chromosome 5. Allele frequency was calculated, excluding any position with missing data. Dataset **#3a** was used.

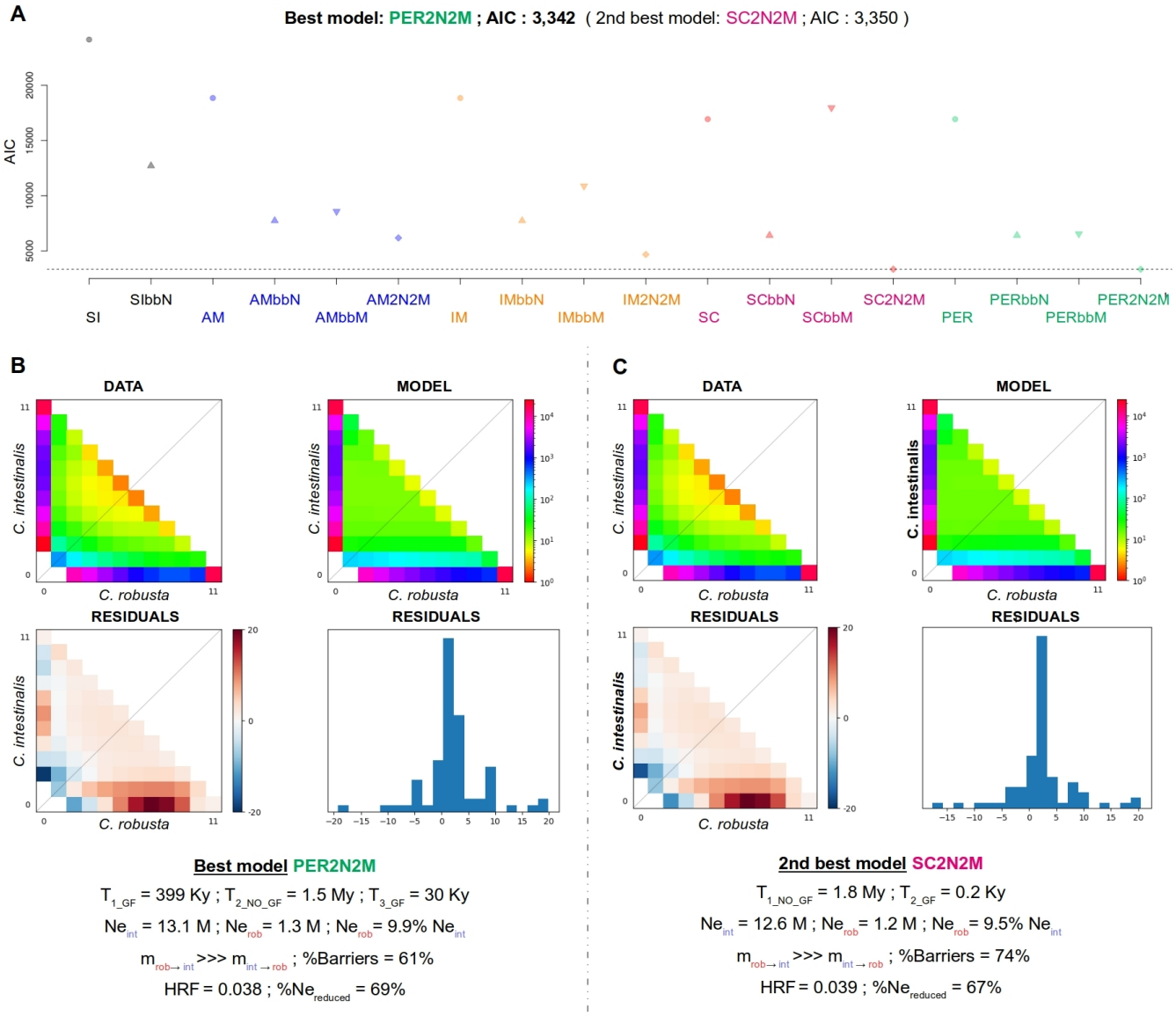

Figure 3 Inference of the divergence history between *C. robusta* and *C. intestinalis* with moments. **A.** AIC value of the best run for each model. **B.** Observed site frequency spectrum (SFS), modeled SFS and residuals of the best model. Maximum likelihood values of the parameters are provided. **C.** Same as in **B** but for the second-best model. Analyses were based on the folded SFS after LD-pruning the SNPs. Five demographic scenarios were modeled: SI = strict isolation, IM = isolation with continuous migration, SC = secondary contact, AM = ancient migration, PER = periodic connectivity. Different versions of these scenarios were tested: bbN = genomic heterogeneity of the effective population sizes, bbM = genomic heterogeneity of the effective migration rates, 2N2M = both types of heterogeneities, “” = no heterogeneities. Five replicates were run for each model. Parameters are as follows: T = times in years, assuming two generations per year in European waters (the “GF” label refers to gene flow), Ne = effective population sizes in numbers of individuals, m = migration rates (direction given by the arrow), %Barriers = proportion of the genome with null migration, $\%Ne_{reduced}$ = fraction of the genome experiencing reduced Ne, HRF = factor by which Ne is reduced. Full details are provided in **Table S3**. Dataset **#5** was used, excluding chromosome 5.

881 **Figure 4** Analyses of the introgression hotspot on chromosome 5. **A.** Maximum F_{ST} between *C. robusta* and *C.*
882 *intestinalis* was calculated in non-overlapping 10 Kb windows along chromosome 5. Windows with less than 10
883 SNPs were excluded. The x-axis is in bp. **B.** Haplotypes of the *C. intestinalis* individuals in the two sampled
884 localities (sample IDs are depicted on the right, see **Table S1**). Each individual displays two haplotypes
885 delimited by horizontal lines. The *C. robusta* introgressed tracts are shown as red bars. The white background
886 represents the non-introgressed tracts and missing data. The tract boundaries were determined based on the
887 ancestry probability of each position, as shown in **Figure S7**. **C.** Frequency of the *C. robusta* alleles lying on the
888 introgressed tracts along chromosome 5. Allele frequency was calculated, excluding any position with missing
889 data (e.g. the nearly fixed SNP at position 28,801 bp on panel **B** was excluded and designated with the first cross
890 on panel **C**). The grey horizontal band running through all panels refers to the "missing data region" (due to high
891 coverage) in the core region of the hotspot (from 1,009,000 to 1,055,000 bp). **D.** Linkage disequilibrium pattern
892 between the 111,951 SNPs fixed between *C. robusta* and *C. roulei*. The color scale indicates the level of LD
893 from blue (low) to red (high). **E.** Haplotype-based selection test using *SelScan*. EHH is shown for the *C. robusta*
894 haplotype (red) and the other haplotypes (black) in *C. intestinalis* (upper panel) and *C. roulei* (lower panel) using
895 a 100 Kb maximal extension. A separate analysis was done on the left and right of the "missing data region"
896 (grey band) using the most frequent *C. robusta* allele closest to the grey band as target SNP. Absolute iHS was
897 calculated based on the EHH results and normalized in windows of 50 Kb. The threshold value of the normalized
898 iHS was set to 3 (which refers to the 99th quantile). Dataset **#2** was used for the F_{ST}, **#3a** for Chromopainter
899 haplotypes and **#4** for the LD triangle.

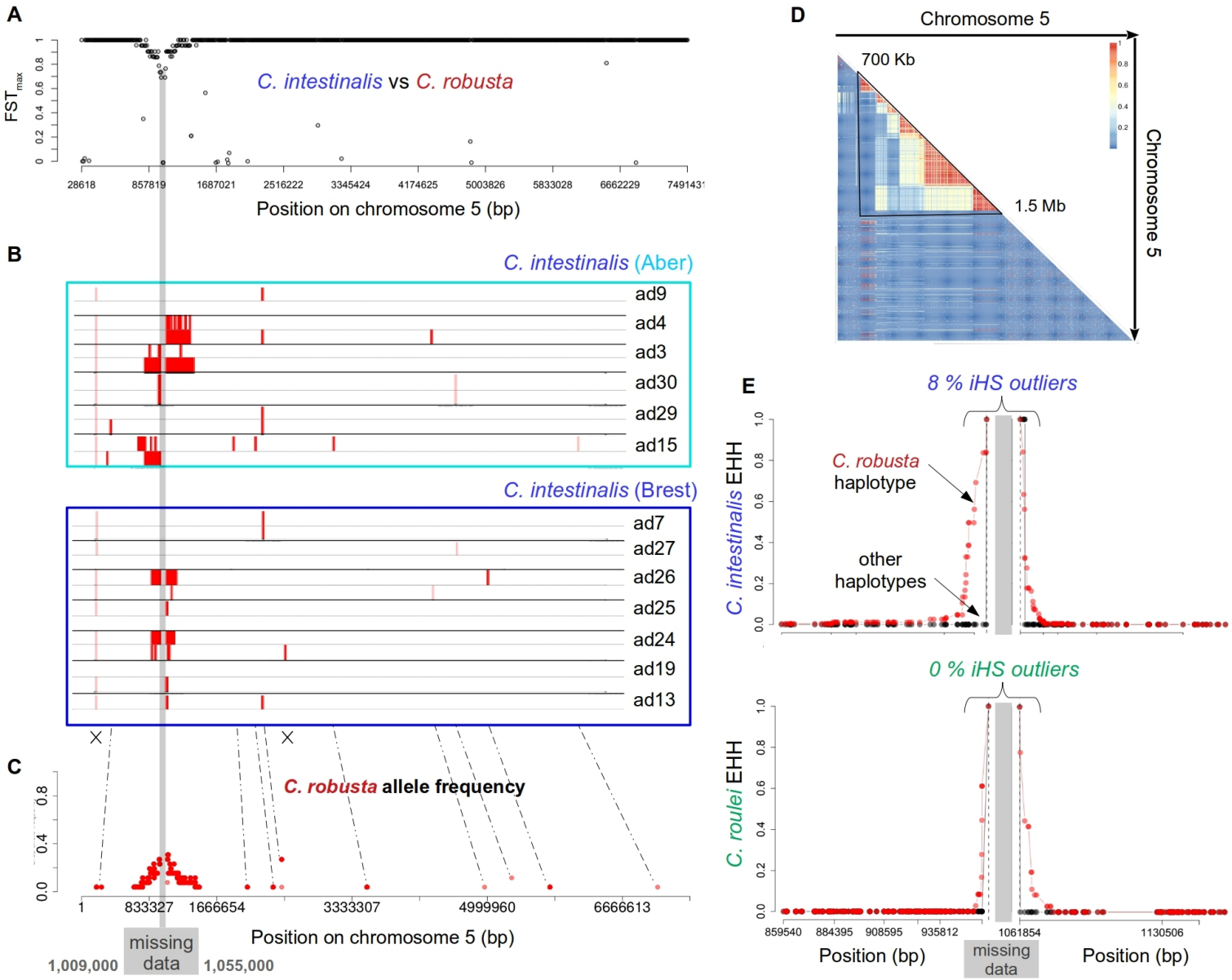
A
FST max
C. intestinalis vs C. robusta
28618
857819
1687021
2516222
3345424
4174625
5003826
5833028
6662229
Position on chromosome 5 (bp)
B
C. intestinalis (Aber)
ad9
ad4
ad3
ad30
ad29
ad15
C. intestinalis (Brest)
ad7
ad27
ad26
ad25
ad24
ad19
ad13
C
C. robusta allele frequency
1
833327
1666654
3333307
4999960
6666613
missing data
1,009,000
1,055,000
Position on chromosome 5 (bp)
D
Chromosome 5
700 Kb
1.5 Mb
Chromosome 5
E
8 % iHS outliers
C. intestinalis EHH
C. robusta haplotype
other haplotypes
0 % iHS outliers
C. roulei EHH
859540
884395
908595
935812
1061854
1130506
Position (bp)
missing data
Position (bp)
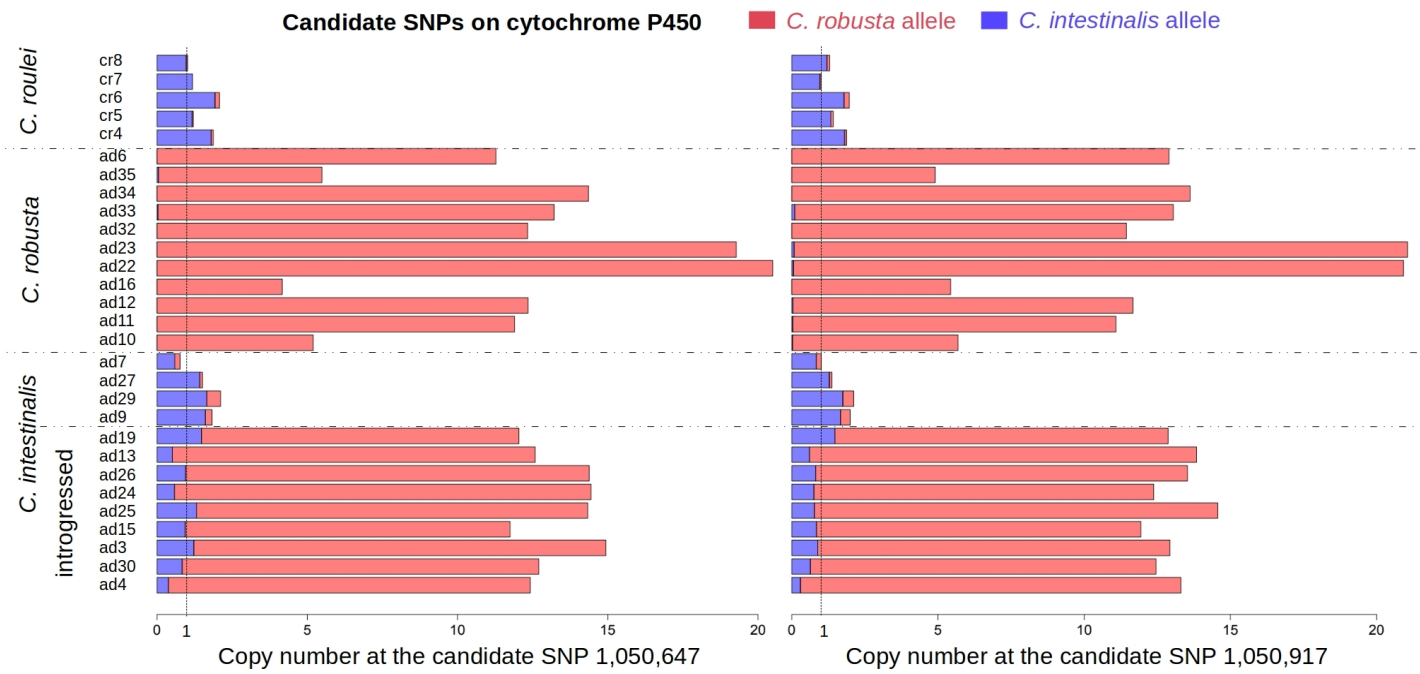
Figure 5 Copy number variation at two candidate SNPs on the cytochrome P450 family 2 subfamily U gene. The two SNPs (labeled with their position in bp) lie in the "missing data region" of the introgression hotspot on chromosome 5. Candidates were defined as having a variant allele fraction, VAF <= 50% in *C. intestinalis*, a VAF >= 90% in *C. roulei* and a VAF <= 10% in *C. robusta*. No candidates were found in the other direction (i.e. with the minor VAF in *C. roulei*). Copy number at each SNP was calculated as its allele read depth normalized by the per-site read depth averaged across all sites (excluding sites with less than ten reads) for each individual (labeled on the left). A copy number of one (vertical dashed line) means that the SNP lies on a single-copy locus. Values for the *C. robusta* allele (red) and the *C. intestinalis* allele (blue) are separately shown. Read depth was obtained from the bam files. Horizontal dashed lines separate the different species, and *C. intestinalis* individuals introgressed at the hotspot (see **Figure 4**) were labeled as "introgressed". Dataset **#7** was used.